



Temperature-Step Electrochemical Impedance Spectroscopy Analyses Ion Conduction Mechanism in Quasi-Solid Semi-IPN Polymer Electrolytes

Dr. Nimai Bar

Department of Chemistry, Natural and Applied Science Research Centre, Raja Narendra Lal Khan Women's College (Autonomous), Vidyasagar University, Paschim Medinipur, Pin-721102

ARTICLE INFO

Received:05.04.2024;

Revised:10.07.2024;

Accepted:12.07.2024

Key Words:

Solid polymer electrolytes (SPE), semi-interpenetrating polymer networks (Semi-IPNs), electrochemical impedance spectroscopy (EIS), Nyquist plots, universal power law (UPL).

ABSTRACT

This ionic transport mechanism for a new class of semi-IPNs polymer electrolytes is probed in considerable detail using temperature-step electrochemical impedance spectroscopy (EIS). The normalized Nyquist plots (Z' vs Z'') shows two well defined regions. One at mid-/high- frequency for bulk and other one is at low frequency is interfacial impedance. Further analysis shows participation of three components contributes in the bulk resistance. Rigorous electrochemical impedance analysis indicates presence of three microscopic phases in the matrix bulk ($R_{\text{PEO-PU}}$, $R_{\text{PEO-PU/PEGDME}}$, R_{PEGDME}) along with the charge transfer resistance (R_{ct}). Debye plots complex impedance against frequency (Z'' vs $\log f$) provides the bulk relaxation time (t_{peak}). The real component of conductivity as function of frequency ($\sigma'(w)$ vs $\log f$) follows universal power law and simulated fit results reveals vital information on the relaxation rate and predominant charge carrier type. Dielectric profiles provide insights into the ion polarization processes. The conductivity of electrolytes matrix elucidated by *ac*-impedance spectroscopy study was further analyzed using simulated model fit to extract pertinent information relevant to the phase composition and homogeneity, contribution of each phase, interfacial charge transfer resistance, phase entanglement zones, relaxation time and ionic hopping mechanisms, associated segmental motions, site-relaxation times and ionic transport numbers. These trends were further correlated with our prior evaluation of the physico-chemical properties of these matrices to propose a rational model for these complex systems.

Introduction

1.1. Background

The need of the hour is to provide solutions for tapping environmentally green sustainable energy resources not only to meet the ever-expanding demands but also to reduce the carbon footprint that is now undeniable.¹⁻⁴ The persistence of environmental protection agencies in developed countries, steep goals set at the Kyoto treaty to regulate greenhouse gas emissions, the increased sense of energy security requirement in developing countries with rapidly expanding economies that rely heavily on fossil fuel imports, universal realization of depleting resources, all have contributed as major drivers for effecting alternate policies, planning and strategies. This global urgency has translated into intensive research to engineer devices that efficiently harvest and store energy from sun, wind, and geothermal or environmentally benign alternative fuels. In this endeavor, two approaches in particular, (i) excitonic solar cells as energy conversion/generation device and (ii) Li-ion rechargeable batteries for efficient energy storage/delivery vehicle, both, have received considerable attention.⁵⁻⁷

Excitonic solar cells, based on organic and/or hybrid materials, have already emerged as an attractive and powerful option to conventional PV technology, based on either silicon or other inorganic semiconductors.⁸ The estimated production

cost of ESCs currently stands in the range 1-2.3\$/watt, with certified efficiencies exceeding 11%, thus comparable to those for commercially available conventional PV modules (e.g. *a*-Si).⁹ Nevertheless, quite a few bottlenecks still remain in the way towards realizing their commercialization. Primarily, availability and price for some of the materials, production costs and device stability are the points of concern. Recent concerted efforts of the academia, research institutions and industries however, have already shown great promise and significant advances to address these issues. A production cost below 1\$/installed watt, with ~7% module efficiency and ~5000hrs of durability is expected to provide acceptable grid parity and allow rapid deployment.¹⁰⁻¹¹

Concurrently, over the last two decades, there has been phenomenal advancement in the Li-ion rechargeable battery technology.¹² The research primarily driven by the automotive transportation sector, space technology and defense need of the developed nations, warranted product reliability. Several research breakthroughs in high capacity and high-power density electrodes, exceptional improvement in recharging at high C-rates, increased shelf-life, performance and safety, all ensured commercial production by major players in the market. Barring a few issues primarily owing to the electrolytes used, such as, electrolyte stability, electrolyte-imposed

design limitations, materials and production costs, the Li-ion battery can contest as a fully matured technology for the future. Estimates by the US-DOE Vehicles Technology program observes that a ~70% reduction in the present manufacturing cost, a ~3.5 times increase in battery life and a ~35% decrease in battery weight can provide competitive advantage to the HEV, PHEV, PEV manufactures and other commercial appliances.

A reliable and reasonably cost-effective solution for these two technologies as briefed above, *i.e.*, an efficient power generation device or a storage/delivery device is especially attractive for stand-alone power generation and distribution in difficult to reach places.¹³⁻¹⁵ In the Indian context, a combination of this option is already being aggressively pursued under the national mission, where rural electrification is severely impeded by the challenges in reaching out to remote areas, yet sunlight is quite abundant. A success in bringing down the materials and manufacturing costs further would ensure rapid deployment that promises huge impact and benefits on the societal and economical fronts.¹⁶⁻²³

1.2 Significance

One of the key constituents in multi-component systems such as, rechargeable batteries, dye sensitized solar cells (DSSC), and several of the envisaged smart devices is the '*electrolyte*'.²⁴⁻²⁶ In such systems,

apart from all the other parameters related to electrodes, dyes, catalysts, etc., the device performance and life-time is dominated by the functioning and stability of the electrolytes under operational conditions. Over the years, electrolyte research has evolved to satisfy the requirement of the industry as well as consumers in both stationary and portable applications.

A long-standing goal in polymer electrolyte research is the preparation of an ideal electrolyte that combines the processing characteristics of conventional thermoplastics and the ionic conductivity of low molar mass liquids. PEs contrast sharply compared to the usual electrolyte materials with respect to the mode of charge transport and the value of ionic conductivity; however, for electrochemical applications the flexibility offered by the polymer electrolyte is important. Coupled with high volumetric power densities, the volume changes in a cell during cycling can be easily accommodated without physical degradation of the interfacial contacts, thus allowing space-efficient battery designs.²⁷⁻³⁰ Though the polymer electrolytes are projected to address multiple issues related to device performance, factors such as relatively low ionic conductivity, the ability of polymer electrolytes to operate with highly reactive electrodes such as lithium over a wider temperature range without deterioration in the charge capacity and electrolyte

properties, the high interfacial electrode-electrolyte impedances are still a major technological challenge and far from practical realization. The present work focuses on the development of improved polymer/polymer-nanocomposite electrolytes as for rechargeable lithium batteries and excitonic solar cells. The project objective entails design, synthesis and detailed physico-chemical and electrochemical property evaluation of functional polymers and polymer / nanocomposites with controlled architecture / morphology. The globally competitive benchmarks for the polymer / polymer-nanocomposite electrolyte matrices are identified as: **1) Li⁺-ion conductivity (σ) > 10⁻³ S/cm; 2) Operating Temperature Range: 20 °C – 80 °C; 3) Thermal Stability: > 150 °C and 4) Shelf-Life > 5 years and are targeted initially.** ³¹⁻³⁸

1.3 Objectives

Polymer electrolytes (PEs) have remained the subject of intensive research since the late seventies with multiple advantages envisaged that can possibly have huge impact on the stability, performance, design and safety of next generation electrochemical devices. Meeting the targeted specifications for practical applications are understandably quite challenging primarily owing to the sluggish dynamics of the macromolecular medium. Over the years, attempts by several research

groups have considerably enriched the field and narrow down on the pre-requisites of such systems. In continuation to our persistent efforts, we have recently reported on a new series of semi-interpenetrating polymer network (semi-IPN) compositions with comprehensive discussion on the effects of (i) constituent composition, (ii) crosslink density, (iii) macromolecular chain length between crosslinks, (iv) molecular weight of the secondary component, (v) charge carrier concentration and (vi) nature of anion on the matrix properties. Encouragingly, bulk ionic conductivities of 10⁻⁴-10⁻³ Scm⁻¹ is observed in a temperature window of 20 °C-80 °C for the optimized semi-IPN system. It is a significant milestone achieved for a quasi-solid polymer matrix, particularly in the absence of any external plasticization. ³¹⁻³⁸

Ionic conductivity in these systems occurs primarily in the amorphous regions and is associated with both the charge migration of ions between coordination sites (ionic hopping) and the polymeric chain segmental motions (micro-Brownian motions). The dynamic bond percolation theory developed by Ratner et al. explains the charge migration in such systems in terms of a renewal of hopping probabilities. Monte Carlo (MC) simulations and the molecular dynamic (MD) approach on both crystalline and amorphous PEO-salt complexes have helped in establishing theoretical models to

explain the mechanism responsible for ionic conductivity.³⁹⁻⁴⁰ Furukawa et al., while making use of a combination of theoretical modelling and accurate measurements of complex conductivity spectra for PPO/(LiClO₄)_x complexes, proposed that the conductivity takes place via two phenomena. The primary objective of the study put forth in this paper is to enhance our understanding of (i) the microscopic molecular events related to the charge transport mechanism, (ii) the correlated motions of the ions and chain dynamics, (iii) the identification of the polarization mechanisms and the relaxation processes, and (iv) the effect of micro-phase separation on such events in these semi-IPN systems. We anticipate that such a detailed analysis will aid us in the appropriate designing of the semi-IPNs as an efficient SPE for applications such as in batteries that we envisage. In contrast to earlier reports where in low molecular weight polymers below the entanglement limits were used, the semi-IPNs investigated in the present study pose a challenge owing to their inherent complexity. The present effort is an attempt toward explaining the charge transport mechanism making use of the models proposed by Furukawa and Di Noto by suitably modifying them to account for the complexities in a semi-IPN.⁴¹⁻⁴⁴

In the present study, we attempt to consolidate our understanding on the rather complex semi-IPN system focusing on the

mechanisms of ionic charge transport in these complex matrices. This ionic transport mechanism for a new class of semi-IPNs polymer electrolytes is probed in considerable detail using temperature-step electrochemical impedance spectroscopy (EIS). The normalized Nyquist plots ($r\phi$ vs $r\phi\phi$) shows two well defined regions, for bulk (at mid-/high- frequency) and interfacial impedance (at low frequency). Further analysis shows participation of three components contributes in the bulk resistance. Rigorous analysis indicates presence of three microscopic phases in the matrix bulk ($R_{\text{PEO-PU}}$, $R_{\text{PEO-PU/PEGDME}}$, R_{PEGDME}) along with the charge transfer resistance (R_{ct}). Debye plots complex impedance against frequency (Z'' vs $\log f$) provides the bulk relaxation time (t_{peak}). The real component of conductivity as function of frequency ($\sigma'(w)$ vs $\log f$) follows universal power law and simulated fit results reveals vital information on the relaxation rate and predominant charge carrier type. Dielectric profiles provide insights into the ion polarization processes. The conductivity of electrolytes matrix elucidated by *ac*-impedance spectroscopy study was further analyzed using simulated model fit to extract pertinent information relevant to the phase composition and homogeneity, contribution of each phase, interfacial charge transfer resistance, phase entanglement zones, relaxation time and ionic hopping

mechanisms, associated segmental motions, site-relaxation times and ionic transport numbers. These trends were further correlated with our prior evaluation of the physico-chemical properties of these matrices to propose a rational model for this complex system.

2. Experimental: Methodology & Design

2.1 Materials: All the chemicals Castor Oil (CO) (BSS grade), diphenylmethane-4,4'-diisocyanate (MDI) (Merck), poly(ethylene glycol) (PEG, $M_n \sim 400, 1000, 2000, 4000, 8000, 10000, 14000$) (Aldrich), poly(ethylene glycol) dimethylether (PEGDME, $M_n \sim 250, 500, 1000, 2000$) (Aldrich), lithium perchlorate (LiClO_4) (Aldrich), trifluoromethanesulfonate, (Aldrich), N,N-dimethylaniline (DMA) (Rankem), tetrahydrofuran (THF) (Rankem) and acetonitrile (CH_3CN) (S.D. Fine-Chem Ltd, India) used were of reagent grade. Polyethylene glycols and the solvents (THF, CH_3CN) were dried prior to synthesis.

2.2 Synthesis of Semi-IPN Electrolyte Matrices: The process of preparing a typical semi-IPN electrolyte matrix involves, forming a isocyanate terminated pre-polymer by reacting castor oil (-OH value ~ 2.7) with a diphenylmethane-4,4'-diisocyanate (MDI) in requisite amount for one hour using THF as the solvent and nitrogen as inert atmosphere (stage-I). Thereafter the reaction vessel containing the

isocyanate terminated pre-polymer is charged with the polyether macromonomer (PEG, $M_n \sim 4000$) and room temperature catalyst N, N-dimethylaniline (DMA) to initiate the formation of the polymer networks, component-I (stage-II). Concurrently, the component-II, *i.e.* PEGDME ($M_n \sim 500$) having non-reactive end group in the preferred weight % is added within the system to intimately entangle within the growing polymer network. The incorporation of electrolyte salt and/or redox couple of desired concentration, dissolved in a 1:1 solvent mixture of THF/ CH_3CN is also achieved at this stage. The reaction mixture is degassed and vigorous mixing is continued for another 30 minutes, under inert atmosphere, to obtain a uniformly homogeneous viscous mix of an electrolyte composition. Finally, the viscous polymer solution is casted onto a teflon petri-dish, dried at room temperature for 24 hrs followed by curing at higher temperature and inert atmosphere to ensure the completion of isocyanate reaction (at 80 °C for 48 hrs) and obtain the quasi-solid semi-IPN electrolyte matrix. The free standing films so obtained have an average thickness in the range of $\sim 0.06 - 0.08$ cm. The synthesized semi-IPN samples are coded as P4K -PU/P2 in the text with the corresponding composition of component-I and component-II provided in brackets as (60:40), (50:50), (40:60) and (30:70)

indicating the respective weight percentage. Compositions beyond 70 wt% of PEGDME visibly lacked structural integrity and phase homogeneity and hence were not considered under this study. The total -NCO / -OH ratio was maintained 1.2 and EO/Li mole ratio of $\text{LiClO}_4 = 30$.

2.3 Synthesis of Semi-IPN Electrolyte Matrices with Variable Chain Length between Crosslinks and Entanglements:

The semi-IPN architecture were tailored to study the effect of chain length between crosslinks and degree of entanglements by either varying the average molecular weight of the macromonomer used in component-I (PEG) or the component-II (PEGDME) during synthesis while keeping all the other parameters and the electrolyte (LiClO_4) used same. The different molecular weights (M_n) of PEG used in the present study are 400, 1000, 2000, 4000, 8000, 10000 and 14000 in combination with PEGDME of $M_n = 500$. The semi-IPNs of (30:70) weight compositions so formed are accordingly coded as P0.4K-PU/P2, P1K-PU/P2, P2K-PU/P2, P4K-PU/P2, P8K-PU/P2, P10K-PU/P2 and P14K-PU/P2, respectively. Similarly, the different molecular weights of PEGDME (component-II) used in the present study are 250, 500, 1000 and 2000 in combination with PEG of $M_n = 4000$ in component-I. The sample compositions are accordingly designated as P4K-PU/P1, P4K-PU/P2, P4K-PU/P3 and P4K-PU/P4,

respectively.

2.4 Characterization

2.4.1 Electrochemical Impedance Spectroscopy (EIS):

The alternating current (ac-) electrochemical impedance measurements were carried out on a Zahner®Zennium electrochemical workstation controlled by Thales Operational Software. The system was interfaced with a thermostated oven equipped with parallel test channels independently connected to spring loaded Swagelok cells to test the samples at identical conditions. The synthesized semi-IPN electrolyte samples were vacuum dried overnight before carrying out the electrical measurements. Punched circular disc shaped polymer films or quasi-solid samples of surface area $\sim 0.95 \text{ cm}^2$ and thickness $\sim 0.06\text{-}0.08\text{ cm}$ were sandwiched between two 316 stainless steel blocking electrodes with a Teflon spacer of appropriate dimension and loaded in the Swagelok assembly. The spring and Teflon spacer ensured the application of same amount of spring pressure during the sample mounting and throughout the test. The sample holders were placed in the controlled heating chamber to carry out the variable temperature impedance measurements over a range of $\sim 20^\circ\text{C}$ to 90°C at an interval of $\sim 5\text{-}7^\circ\text{C}$ during heating. The temperature was measured with accuracy better than $\pm 0.1^\circ\text{C}$ using a K-type thermocouple placed in close proximity with

the sample. Samples were equilibrated at each temperature for 30 minutes prior to acquiring the frequency sweep impedance data. All data were collected following a frequency sweep through 1Hz to 4MHz range at an alternating potential with a RMS-amplitude of 10mV across the OCV of the assembled cells. No corrections for thermal expansion of the cells were carried out. The real part of the impedance was appropriately normalized for the cell dimensions and ionic conductivity (s (Scm^{-1})) was determined. The model and simulated fits for the Nyquist plots were achieved using Zmann 4.0 Analysis Software. Analysis of temperature dependence of the electrochemical spectroscopy data was done by non-linear least square fits (NLSF) using Microcal OriginPro 8.5 software. The maximum error associated with all the simulated fits is within $\pm 1\%$.

The *dc*-polarization tests were carried out on the same set up as described in the above section at three temperatures of interest ($\sim 30\text{ }^\circ\text{C}$, $50\text{ }^\circ\text{C}$ and $80\text{ }^\circ\text{C}$). The decay of current in response to a constant voltage (1 V) was measured as a function of time (6 h). All the synthesized samples were vacuum dried overnight at $80\text{ }^\circ\text{C}$ before carrying out the characterizations.

3. Results and Discussion

Impedance spectroscopy is a powerful probe to study the structure-conductivity correlations in glassy or solid polymeric

materials.^{33,34} Electrochemical impedance is normally measured by applying an *ac*-potential to an electrochemical cell (SS/PE/SS) and then measuring the current through the cell. In an *ac*-impedance experiment a sinusoidal voltage is applied to a cell and the sinusoidal current passing through the cell as a result of this perturbation is measured. Contrary to the *dc*-conductivity measurements where only one parameter R_b is measured, in the case of an *ac*-perturbation two parameters are required to relate the current flowing in response to an applied potential. One represents the opposition of the system to the flow of charge and is equal to the ratio of the voltage and current maxima, $V_{\text{max}}/I_{\text{max}}$ and is analogous to the resistance in *dc* measurements. The other parameter theta (q) is the phase difference between the voltage and current. The combination of these different parameters represents the impedance (Z) of the cell. Generally, both the magnitude of the impedance $\frac{1}{2}Z^{1/2} = V_{\text{max}}/I_{\text{max}}$ and its phase angle q are functions of the applied frequency. *ac*-impedance measurements were performed between 1 Hz to 4 MHz and the experiments were performed in the temperatures range from 296 K to 363 K. The terminal pair measurement method was adopted using two types of home made Teflon cells. The samples in the form of film were placed between two circular stainless steel 306

electrodes and the electrolyte sample was sandwiched between these two SS electrodes. No corrections for thermal expansion of the cell were carried out.

In the equivalent circuit analog, resistors represent conductive pathways for ion and electron transfer. As such, they represent the bulk resistance of a material to charge transport such as the resistance of the electrolyte to ion transport or the resistance of a conductor to electron transport. Resistors are also used to represent the resistance to the charge-transfer process at the electrode surface. Capacitors and inductors are associated with space-charge polarization region such as the electrochemical double layer and adsorption/desorption process at an electrode respectively. In our polymer electrolytes, for data simulation the inductance of the wires are not considered in the equivalent model. Most of the circuit elements in the model are common electrical elements such as resistor, capacitors, inductors and constant phase elements. Resistors impedance ($R_z=R$), is independent of frequency. But for inductors impedance increases with increasing frequency ($I_z=j\omega L$), for capacitor impedance decreases with increasing frequency ($C_z=1/j\omega L$). To analyze the characteristics of the Nyquist impedance plot, an equivalent circuit is used because it is simple fast, and can provide a complete picture of the system. Detailed analysis of

the Nyquist plots for our semi-IPN electrolyte matrix is initiated by first creating a feasible and realistic model of the bulk using a combination of distributed element that best represents the complex system. As detailed in the schematic representation (**Figure 1**) the four resistance (R_1, R_2, R_3 , and R_{ct}) coupled with four constant phase element (Q_1, Q_2, Q_3, Q_{dl}) and a semi-infinite bound Warburg resistance for the electrode-electrolyte interface (W_o) can be appropriately connected in a combination of parallel and series circuit best mimics the different phases that are expected to be present in the semi-IPN electrolyte matrix.

Following a normalization of impedance spectrum prior to any data treatment, the parameters were iterated about initial values using nonlinear least-square fitting with statistical weighting to obtain the best fit to the data. The fitting proceeded through several iterations in Zmann 4.0 Software. **Figure 2** shows the Nyquist impedance plots for the semi-IPN polymer electrolytes. It is clearly seen that there is a depressed semi-circle in the mid-/high- frequency range and an inclined straight line in the low frequency range for each sample. These plots deviate from an ideal impedance spectrum that usually exhibits a standard semicircle at high frequency section and vertical line at lower frequency section.

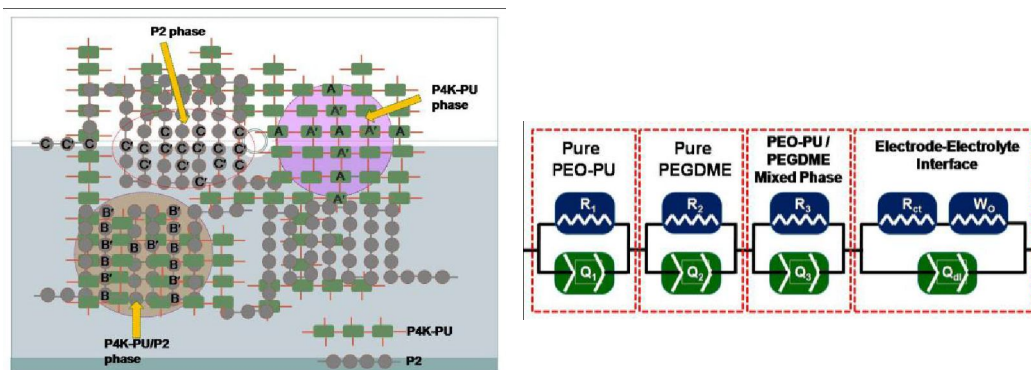


Figure 1. A schematic representation of tri-phasic semi-IPN solid polymer electrolytes matrix and a plausible electrical equivalent circuit represented by the distributed elements.

Following a normalization of impedance spectrum prior to any data treatment, the parameters were iterated about initial values using nonlinear least-square fitting with statistical weighting to obtain the best fit to the data. The fitting proceeded through several iterations in Zmann 4.0 Software. The high frequency range which is related to conduction process in the bulk of the electrolytes and the linear region is the low frequency range that is attributed to the effect of blocking electrodes where diffusion related capacitance at the electrode-electrolyte interface comes into play. The deformed semicircle is dependent on the non-ideal behavior of the matrix, relaxation time associated with ionic hopping, morphology of the polymeric film and the surface-roughness of the electrode. The impedance depends on the frequency of the potential perturbation. For all compositions a slight degree of depression of center has been observed and these effects reveal the

non-Debye nature of material and distribution of relaxation time.

In our polymeric system are mainly polyether based electrolytes where two component system, methoxy (-OMe) capped polymer (PEGDME) interpenetrates into polyurethane (PU) network system. The resulting spectrum is a typically a semicircle and asymmetric in shape due to convolution of three different contributions *i.e.* bulk and grain boundary to the ionic resistance of electrolyte polymer film. The bulk resistance contains three individual component contributions those are overlap with one another resulting bulk resistance, which slightly lower than calculated value of resistance. High resistance due to pure PEO-PU ($R_{\text{PEO-PU}}$) component, low resistance for pure PEGDME (R_{PEGDME}) component and moderate resistance portion due to mix phase of PEO-PU/PEGDME ($R_{\text{PEO-PU/PEGDME}}$). Linear spike of resistance to the imaginary component is assigned for

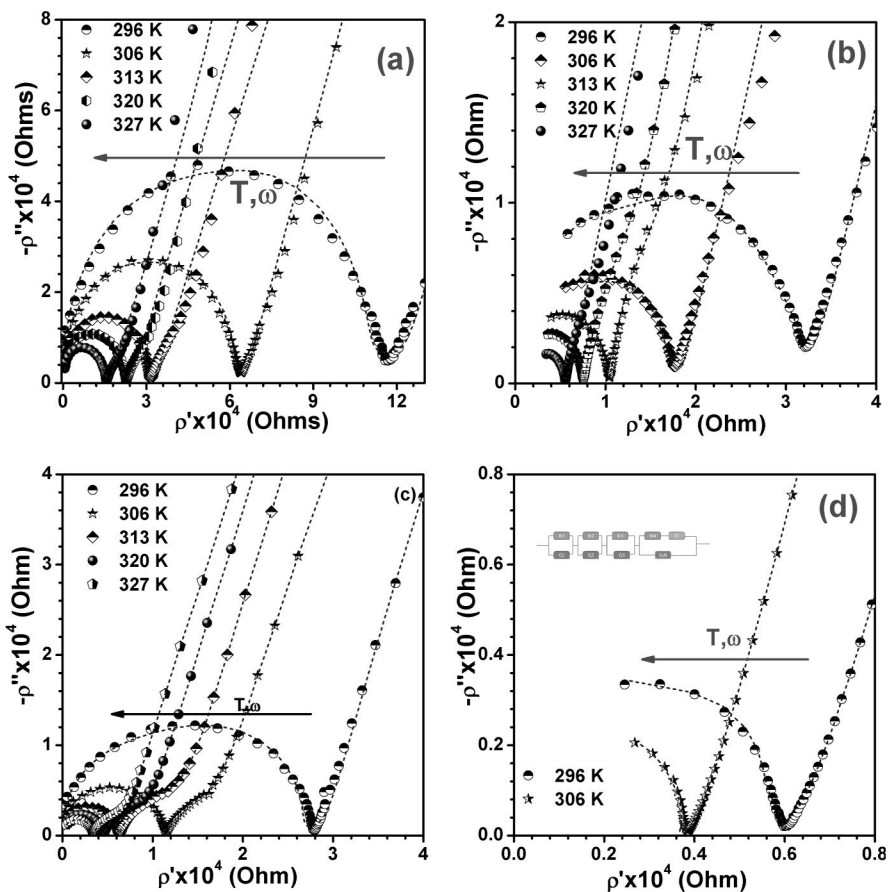


Figure 2. Nyquist plots ($r\phi$ versus $-r\phi\phi$) of selected for the solid polymer electrolytes (SS/PE/SS) complexes at various temperatures and compositions of electrolytes matrix (a) P4K-PU/P2/LiClO₄ (60/40) (b) P4K-PU/P2/LiClO₄ (50/50) (c) P4K-PU/P2/LiClO₄ (40/60) and (d) P4K-PU/P2/LiClO₄ (30/70) at five different temperatures 296 K, 306K, 313 K, 320 K and 327K. For P4K-PU/P2/LiClO₄ (30/70) impedance data fitted up to room temperature at higher temperatures semicircular arc vanishes. The dotted lines indicate the fitted data of the normalized impedance diagram.

the charge transfer resistance (R_{ct}). The bulk resistance strongly depends on compositions of electrolytes matrix, macromonomer chain length and oligomeric entanglements. It has been observed that on increasing the amount of second component (PEGDME) into the polymer electrolytes matrix resistance values of the three microscopic component

decreases as well bulk impedance value decreases. Similar trend is followed in conductivity plots as observed for microscopic component. The corresponding capacitance values do not follow any trend on increasing temperature and compositions but capacitance value for PEO-PU matrix is lowest, mixing phase (PEO-PU/

Table-1: Calculated Values of Resistances obtained from the Complex-Plane plots in the PEO-PU phase (R_{PEO-PU}), PEGDME phase (R_{PEGDME}), and the bulk resistance (R_b), along with the PEO-PU/PEGDME mixed phase ($R_{PEO-PU/PEGDME}$) of the network polymer matrix PEO-PU/PEGDME of different composition, variation with macromonomer and oligomer chain length, studied at 306 K.

Sample Name	R_{PEO-PU}	R_{PEGDME}	$R_{PEO-PU/PEGDME}$	R_{ct}	R_b
P4K-PU/P2 (60/40)	3.67×10^4	4.08×10^3	2.46×10^4	1×10^4	6.3×10^4
P4K-PU/P2 (50/50)	1.02×10^4	4.0×10^3	5.0×10^3	9.0×10^3	1.75×10^4
P4K-PU/P2 (40/60)	6.0×10^3	1.0×10^3	5.00×10^3	1.13×10^4	1.17×10^4
P4K-PU/P2 (30/70)	1.66×10^3	9.85×10^2	1.01×10^3	8.67×10^2	3.4×10^3
P0.4K-PU/P2 (30/70)	5.97×10^3	3.01×10^3	4.0×10^3	4.0×10^3	1.2×10^4
P1K-PU/P2 (30/70)	4.64×10^3	2.34×10^3	2.47×10^3	2.0×10^3	8.5×10^3
P2K-PU/P2 (30/70)	3.81×10^3	2.0×10^3	3.8×10^3	4.80×10^3	8.2×10^3
P4K-PU/P2 (30/70)	1.66×10^3	9.85×10^2	1.01×10^3	8.67×10^2	3.4×10^3
P10K-PU/P2 (30/70)	4.04×10^3	2.0×10^3	3.0×10^3	1.0×10^3	8.7×10^3
P14K-PU/P2 (30/70)	6.5×10^3	2.9×10^3	4.0×10^3	9.7×10^2	1.2×10^4
P4K-PU/P2 (30/70)	1.66×10^3	9.85×10^2	1.01×10^3	8.67×10^2	3.4×10^3
P4K-PU/P3 (30/70)	3.3×10^3	2.0×10^3	2.05×10^3	1.0×10^4	7.1×10^3
P4K-PU/P4 (30/70)	1.4×10^4	9.9×10^3	1.2×10^4	1.0×10^4	3.45×10^4

Table 2. Calculated values of Capacitance obtained from the complex-plane plots in the PEO-PU phase (C_{PEO-PU}) and PEGDME phase (C_{PEGDME}) mixed phase of PEO-PU/PEGDME ($C_{PEO-PU/PEGDME}$) of the network polymer matrix PEO-PU/PEGDME of different composition, variation with macromonomer and oligomer chain length, studied at 306 K.

Sample Name	$C_{PEGDME}(F)$	$C_{PEO-PU/PEGDME}(F)$	$C_{PEO-PU}(F)$	Q_{dl}
P4K-PU/P2 (60/40)	1.88×10^{-7}	1.55×10^{-11}	8.78×10^{-12}	7.36×10^{-1}
P4K-PU/P2 (50/50)	1.71×10^{-6}	1.34×10^{-11}	2.86×10^{-11}	7.44×10^{-1}
P4K-PU/P2 (40/60)	8.85×10^{-7}	7.77×10^{-11}	1.63×10^{-11}	6.73×10^{-1}
P4K-PU/P2 (30/70)	6.45×10^{-12}	6.45×10^{-12}	3.69×10^{-14}	8.06×10^{-1}
P0.4K-PU/P2 (30/70)	2.00×10^{-8}	3.33×10^{-11}	8.29×10^{-14}	8.47×10^{-1}
P1K-PU/P2 (30/70)	1.34×10^{-8}	1.66×10^{-12}	4.94×10^{-13}	6.95×10^{-1}
P2K-PU/P2 (30/70)	3.49×10^{-8}	1.12×10^{-10}	2.16×10^{-13}	7.79×10^{-1}
P4K-PU/P2 (30/70)	3.49×10^{-8}	7.77×10^{-14}	2.08×10^{-14}	8.06×10^{-1}
P10K-PU/P2 (30/70)	6.66×10^{-9}	9.48×10^{-12}	5.98×10^{-11}	7.29×10^{-1}
P14K-PU/P2 (30/70)	2.24×10^{-8}	2.29×10^{-10}	1.23×10^{-11}	7.68×10^{-1}
P4K-PU/P2 (30/70)	6.45×10^{-12}	6.45×10^{-12}	3.69×10^{-14}	8.06×10^{-1}
p4K-PU/P3 (30/70)	1.9×10^{-8}	4.9×10^{-12}	4.1×10^{-13}	7.31×10^{-1}
P4K-PU/P4(30/70)	6.13×10^{-9}	5.59×10^{-11}	2.09×10^{-12}	7.65×10^{-1}

PEGDME) is moderate values and highest capacitance values for PEGDME phase for all the compositions.^{33,38}

Temperature effects the frequency range of the profiles. The three intercepts on real part of Nyquist plots indicates the three-phase resistance ($R_{\text{PEO-PU}}$, R_{PEGDME} , $R_{\text{PEO-PU/PEGDME}}$) and sum corresponds to the bulk resistance (R_b) of the solid polymer electrolytes (SPE). The fitting parameters of equivalent circuit $R_{\text{PEO-PU}}$, R_{PEGDME} , $R_{\text{PEO-PU/PEGDME}}$ (mix), R_b are listed in **Table 1** and corresponding capacitance values ($C_{\text{PEO-PU}}$, $C_{\text{PEO-PU/PEGDME}}$ (mix), C_{PEGDME} and Q_{dl}) are listed in **Table 2**. Three regions are corresponding at low resistance region for pure PEGDME phase, intermediate resistance for PEO-PU/PEGDME mixed phase and high resistance for pure PEO-PU region respectively. Data were obtained in the temperature range 296 K- 327 K.

However, with an increase of temperature, the high frequency semicircle gradually decreases in size and disappear at 335 K.³⁸

The study of dielectric relaxation in solid polymer electrolytes is a powerful approach for obtaining information regarding the characteristics of ionic and molecular interactions. The variation of dielectric constant with temperature is different for polar and non-polar polymers. In general for polar polymers the dielectric constant increases with increasing temperature. But in case of non-polar polymers the dielectric constant is independent temperature. The frequency dependence of dielectric constant (real and imaginary component of dielectric constant) at different temperatures for semi-IPN electrolytes P10K-PU/P2/LiClO₄ sample is shown in

Dielectric constant (ϵ') is a measure of reduction of coulomb interaction between

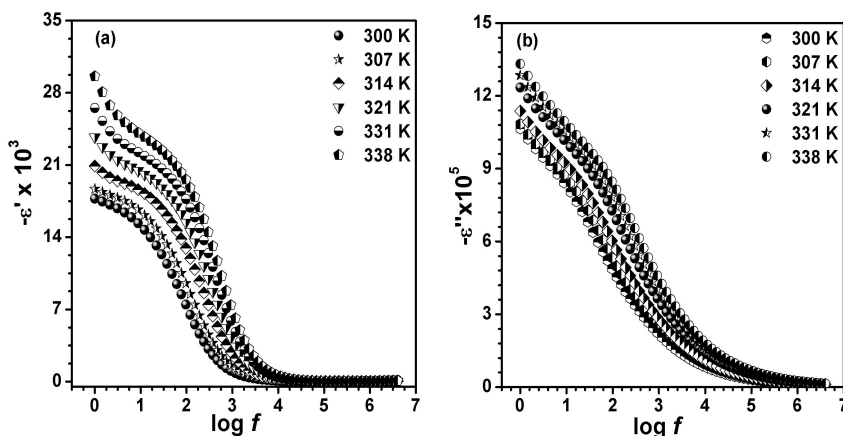


Figure 3. Variation of dielectric constant (ϵ') with frequency at different temperatures for P10K-PU/P2 semi-IPN electrolytes matrix, **(a)** real component of dielectric constant (ϵ') against $\log f$ and **(b)** for the imaginary component of dielectric constant (ϵ'') vs $\log f$ at different temperatures.

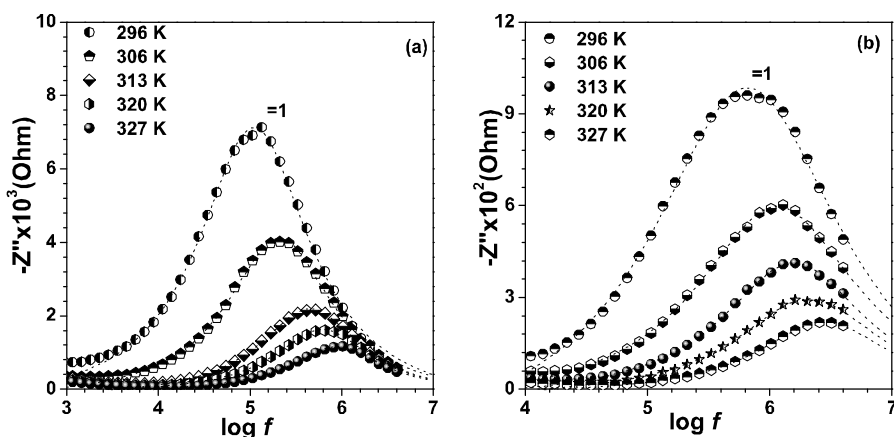


Figure-4. Imaginary component of complex impedance, $-Z''\phi(\omega)$ versus $\log f$ of (a) P4K-PU/P2/LiClO₄ (60/40) and (b) P4K-PU/P2/LiClO₄ (50/50) at five different temperatures like 296 K, 306 K, 313 K, 320 K and 327 K. The short dashed lines indicates the Lorentzian function fit for the Debye plots.

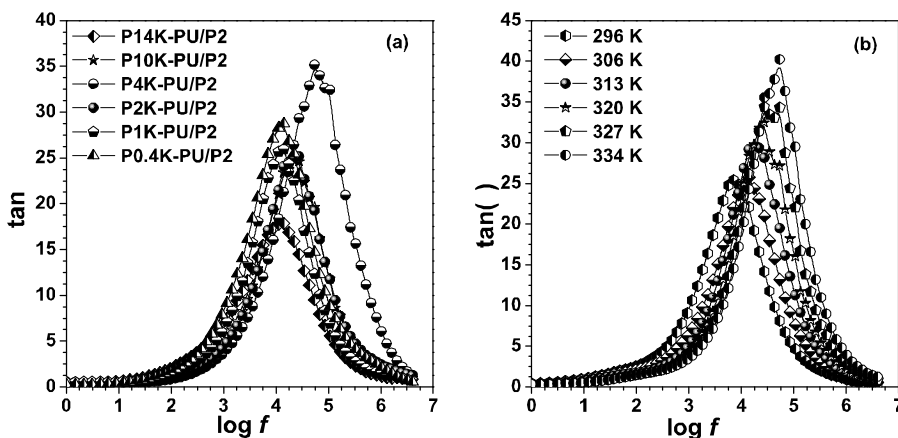


Figure 5. Representative plots of $\tan(\delta)$ against frequency. (a) the typical stack plot $\tan(\delta)$ vs $\log f$ for the P_xK-PU/P2 solid polymer composites containing various molecular weight of macromonomer and (b) plots of the semi-IPN P10K-PU/P2 at different temperature; where $\tan(\delta)$ calculated by real part of dielectric constant vs complex part of dielectric constant (ϵ'/ϵ'').

the ion pairs in the polymer electrolyte matrix. This dielectric property provided valuable information such as characteristic of the ionic/molecular interaction of the polymer electrolyte and the understanding of ion transport behavior as well. It can be clearly seen that the values of ϵ' and ϵ'' as increase

frequency. Here, in **Figure 3** clearly indicates, two distinct phenomenon has been observed, the decrease of dielectric constant value at lower frequency region sharply falls but slowly decreases at higher frequency region. The decrease in dielectric permittivity with increasing frequency can

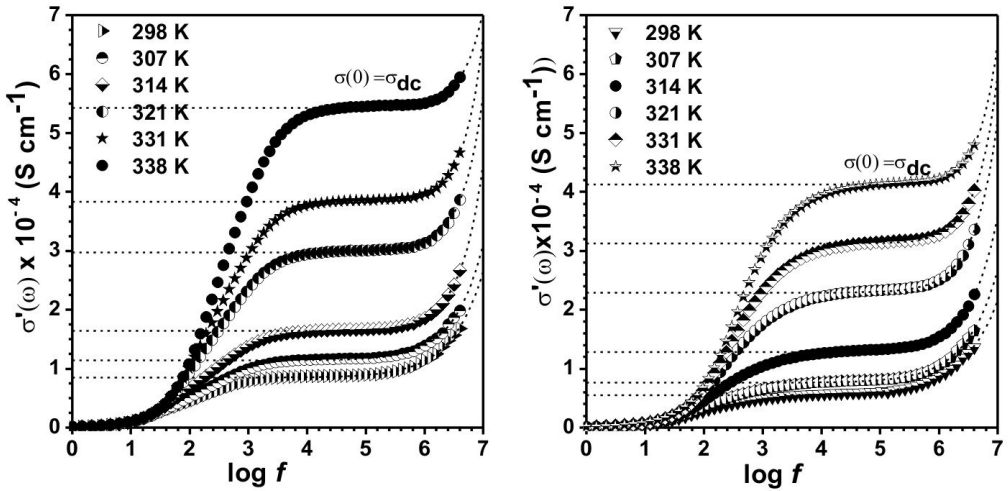


Figure 6. Real component of conductivity $\sigma'(\omega)$ versus $\log f$ (a) for the P10K-PU/P2 (30/70) doped with LiClO_4 at different temperature and (b) for the P14K-PU/P2 (30/70) doped with LiClO_4 at various temperature.

be associated to the inability of dipoles to rotate rapidly leading to a lag between frequency of oscillating dipole and that of applied field. The τ lies in the range of $2.2 \times 10^{-3} \sim 1.5 \times 10^5$, at room temperature. Such high dielectric constant values in our sample can be attributed to high ionic conductivity on account of the presence due to the good interactions between the Lewis acidic sites of the ethylene oxide unit ($-\text{CH}_2-\text{CH}_2-\text{O}$) and the ions of the lithium perchlorate. When the temperature is raised, dielectric constant also enhances due to the facilitation in orientation of dipoles within the semi-IPN matrix of P10K-PU/P2/ LiClO_4 . In all the cases, the increase in dielectric constant implied the increase in the number of ions.

When an electric field is applied to solid

polymer electrolytes polymer films, the charge moves through PEO-PU phase, which is a relatively more conducting phase but are interrupted as the charge comes across the highly resistivity PEGDME phase. The plots of $-Z''(\omega)$ vs the logarithms of frequency $\log(f)$ reveal the presence of typical Lorentzian peaks which shifts to higher frequencies with increasing temperature. On increasing temperature intensity of the peak FWHM decreases. The Debye peak observed when the condition $\omega\tau=1$ is satisfied, where ω is the angular frequency ($\omega = 2\pi f$) and t_{peak} is the Debye relaxation time. **Fig 5** shows that the frequency of the maximum of these Lorentzian shapes depends on the polymer electrolytes matrix composition, temperature. Fitting these profiles by

Lorentzian functions allowed us to measure t_{peak} at the maximum height of the peaks and to establish the relationship between the conductivity relaxation times $t_{\text{peak}} = 1/f_{\text{peak}}$ and both the temperature and the composition of the semi-IPN solid polymer electrolyte matrix.^{45, 46}

Figure 5 shows the variation of tangent loss with different frequencies. The tangent loss spectra were characterized by peak appearing at a characteristic frequency for the samples fabricated in different environments showing the presence of dipoles relaxation in the polymer electrolyte samples. It was evidenced that good combination in increased amorphous nature of the materials with optimum amount of free ionic charge carriers thereby increased the segmental motion of polymer and enhanced the ion transport properties as the peak shifted to higher frequency side. Whereas in Debye plot (**Figure 4**) imaginary vs frequency shows similar trend *i.e.* with increasing temperature FWHM of Debye peak reduces and peak shifted to higher frequency region. The entire frequency dependent diagram offers that on increasing temperature peak shifted on the road to higher frequency region similarly at high frequency region ionic transport mechanism is faster than low frequency region.

Statistical weighting is necessary, since the data span several orders of magnitude,

both in s and in w . Ionic conductivity (s) of solid polymer electrolytes as a function of frequency. Frequency dependence of conductivity spectrum exhibits three distinguishable regions (*a*) low frequency dispersion, (*b*) an intermediate frequency plateau and (*c*) an extended dispersion at high frequency. The variation of conductivity in the low frequency region is attributed to the polarization effects at the electrode and electrolyte interfaces. As the frequency reduces more and more charge accumulation occurs at the electrode and electrolyte interface and drop in conductivity. In the intermediate frequency plateau region conductivity is almost found to be frequency independent and is equal to dc conductivity s_{dc} . In the high frequency region the conductivity increases with the frequency. The frequency dependence of conductivity or so called universal dynamic response of ionic conductivity is related by a simple expression given by Jonscher's power law.^{47, 48}

By making use of the impedance data and the equation

$$\sigma'(\omega) = Z(\omega) / k[(Z'(\omega))^2 + (Z''(\omega))^2] \dots \dots (1)$$

Where k is the cell constant in centimeters, we calculated the real component of the conductivity $s\ell(\omega)$. The $s(\omega)\ell$ spectra of polymer electrolyte samples are shown in below **Figure 5**, with simulated form. These

profiles are characterized by three different regions: **(a)** the low frequency spike, **(b)** the medium frequency plateau, and **(c)** the high frequency spike. The steep increase in $s\omega(\omega)$ at high frequencies was attributed to correlated ionic motions in the solid polymer electrolytes bulk materials.

$$\sigma(\omega)' = \sigma'(0)[1+(\omega\tau_1)^p] \dots \dots \dots (2)$$

According to jump relaxation model which takes account of the Coulomb interaction between mobile ions; p in equation (1) means the ratio.

$$p = \text{backhop rate} / \text{site relaxation}$$

The fact that $0 < p < 1$ implies that the back hop is essentially slower than the site relaxation. The back-hop is the backward motion of a hopping ion its initial site, which is caused by the Coulomb repulsive interaction between mobile ions. The site relaxation is the shift of a site potential minimum to the position of the hopping ion, which is caused by a rearrangement of neighboring ions. The enhancement of the Coulomb interaction between the mobile ions with increase their concentration would raise the back-hop rate and/or lower the site relaxation rate, leading to increase in p .⁴⁹

In our previous report, Basak *et al.* clearly stimulated two fittings in the UPL equation. Where in UPL fitted provide ion dynamics in PEO-PU and PAN phase respectively, two site relaxation energy height barrier for the two phases (E_a , PEO-

PU and E_a , PAN). The activation energy for PEO-PU phase is lower than PAN phase *i.e.* PAN phase is important factor in the conduction mechanism. In concurrent report where stimulated fit of UPL curves provides single fit one relaxation times obtained for the polymer electrolytes matrix, dc conductivity ($s(0) = s_{dc}$) successively increases with increasing temperature and relaxation times (t) decreases but exponent value not follows sequence. Our system is composed of biphasic system where two components are ether based where two component are compactible well behaves as single component system.

It is observed that the frequency at the dispersion region deviate from the dc conductivity plateau is defined as characteristics frequency (ω_p) and also known as the hopping rate, at which $s_w = 2s_0$. The relation between the dc conductivity and hopping rate is given by $s_0 = k\omega_p$ where k is the empirical constant which depends on the concentration of mobile ions and the conduction mechanism. The frequency dispersion region starts to decrease and disappear with increase in temperature. Thus the hopping rate (ω_p) at which the relaxation effects begin to appear moves towards the higher frequency with increasing temperature. The frequency independent conductivity is due to the long range transport of the mobile lithium ions in the response to the electric field, where only

Table 3. Parameters $s(0) = s_{dc}$, Relaxation Time (τ) and Frequency Exponent (p) obtained from the Universal Power Law (UPL) Fits for the PEO-PU Phase of the $P_xK\text{-PU}/P_n/LiClO_4$ semi-IPN solid polymer electrolytes matrix at 306 K. * The double dash line (—) indicates for the selective compositions where UPL equation not applicable.

Sample Name	$\sigma(0)_{PEO-PU}$	$\tau_{PEO-PU(s)}$	P_{PEO-PU}
P4K-PU/P2 (60/40)	1.51×10^{-5}	2.83×10^{-8}	0.5
P4K-PU/P2 (50/50)	5.28×10^{-5}	1.74×10^{-8}	0.68
P4K-PU/P2 (40/60)	8.44×10^{-5}	6.18×10^{-10}	0.35
P4K-PU/P2 (30/70)	--	--	--
P0.4K-PU/P2 (30/70)	7.78×10^{-5}	1.48×10^{-8}	0.55
PK-PU/P2 (30/70)	1.06×10^{-4}	2.7×10^{-8}	0.53
P2K-PU/P2 (30/70)	1.18×10^{-4}	1.60×10^{-8}	0.59
P4K-PU/P2 (30/70)	--	--	--
P10K-PU/P2 (30/70)	1.09×10^{-4}	2.3×10^{-8}	0.83
P14K-PU/P2 (30/70)	7.51×10^{-5}	6.68×10^{-8}	0.88
P4K-PU/P3 (30/70)	--	--	--
P4K-PU/P4 (30/70)	--	--	--

successful jumps contribute to the yielded dc conductivity s_0 . The lower value of p **Figure 7(a)** could be attributed to a higher rate of successful jumps and in turn result in higher dc-conductivity. The value of p as a function of temperature can be directly related to the existence of range of relaxation parameters of mechanism and the magnitude of p contributes to the measure ac conductivity.

Information about ion conduction mechanism in the polymer electrolytes system, is studying by conductivity relaxation times. The conductivity relaxation time determined from Debye peaks and from UPL fit of $s\phi(\omega)$ vs $\log f$ respectively. The relaxation time indicates faster chain

dynamics in the polymer electrolytes matrices. The analysis of these relaxation times as presented in **Figure 7(b)** show typical Arrhenius behavior.

$$\tau = \tau_0 \exp(-Ea/kT) \dots \dots \dots (3)$$

This result indicates that polymer chain dynamics and free charge carriers regulates the conductivity in the polymer electrolytes matrices.

For polarization studies, cells were constructed by sandwiching the solid polymer film between symmetrical stainless-steel electrodes (SS/PE/SS) and the experiment was performed at room ambient for the polymer electrolytes matrix of compositions P0.4K-PU/P2/LiClO₄, P4K-PU/P2/LiClO₄, P10K-PU/P2/LiClO₄

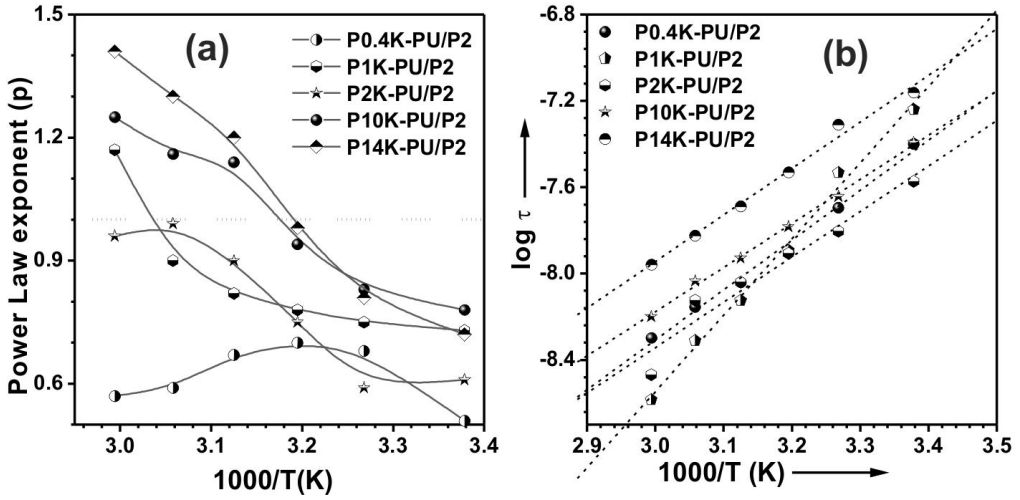


Figure 7. Representative plot of (a) power law exponent, p as a function of temperature and (b) $\log \tau$ vs $1000/T$ plots of conductivity relaxation time (t_{peak}) for the samples. The dotted lines in (b) represents the Arrhenius fit.

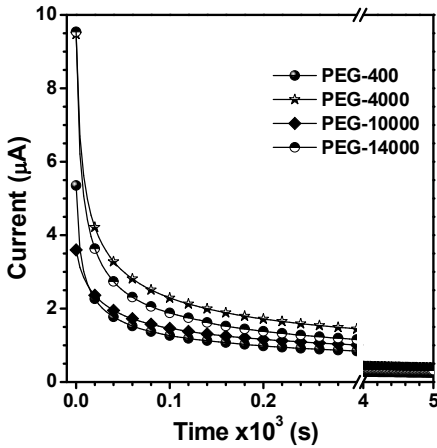


Figure-8 Representative current as a function of time plots for $P_xK\text{-PU/P2}$ sample (where $x=400, 4000, 10000$ and 14000) of different PEG molecular weight to estimate ionic contribution (t_{ionic}) in the polymer electrolytes matrix. The solid polymer electrolytes matrix sandwiched between two spring-loaded stainless-steel blocking electrodes held at constant 1 Volt for the ac -polarization test.

and $P14K\text{-PU/P2/LiClO}_4$. Movement of charge through solid polymer electrolytes matrix generally ionic in nature. Ideal electrolytes for alkaline metal ion batteries, transport number of cations should be high.

Transport number is one of important parameter for the conduction behavior of the solid polymer electrolytes matrix. It has been observed from **Figure 8** that the current initially falls down rapidly and then

attains a constant decay after half an hour. Approximate values of the ionic ($t_i = t_a + t_c$) and electronic transport (t_e) number can be estimated from the polarization curve using the equations:

$$t_i = (I_i - I_r) / I_i \dots \dots \dots (1)$$

$$t_e = 1 - t_i \dots \dots \dots (2)$$

Where, I_i is the initial current and I_r is the residual current. For the semi-IPN compositions of various macromonomer molecular weight (PEG- M_n) the ionic transport lies within the 0.92 ± 0.02 and electronic transport number lie within 0.08 ± 0.02 correspondingly at working temperature. The resulted transport number indicates that ion conduction through the polymer electrolytes matrix is mainly ionic in nature, polymer segmental motion and ion mobility is high within the polymer matrix.⁵⁰⁻⁵²

It has been observed that ionic transport number for the semi-IPN solid polymer electrolytes increases with increasing macromonomer chain length after certain chain length of macromonomer transport number decreases. Maximum transport number obtained for the polymer electrolytes matrix for P4K-PU/P2. Higher molecular weight containing electrolytes matrix due to repletion of ethylene oxide ($-\text{CH}_2-\text{CH}_2-\text{O}$) crystallinity within the matrix is higher. For low molecular weight macromonomer due to transient cross-link between ether oxygen

group and lithium metal ion (Li^+) restrict the ionic motion as a result ionic conductivity decreases which proves in our earlier report.

4. Conclusion

Polymer electrolytes (PEs) are projected to address multiple issues related to ease of processing, leakage and evaporation, impart flexibility in design and weight, increase device performance, enhance life-time, issues pertaining to safety with all solid state Li-ion batteries and provide affordability and cost-competiveness to the delivered product. Nevertheless, factors such as relatively low ionic conductivity, the ability of polymer electrolytes to operate with highly reactive electrodes such as lithium over a wider temperature range without deterioration in the charge capacity and electrolyte properties, the high interfacial electrode-electrolyte impedances, adhesion, lamination and wetting are still major technological challenges and far from practical realization.

- Success of the proposed program can take us a giant step forward towards achieving all solid state Li-ion Batteries, ease of processing, impart flexibility in design and weight, increase performance, enhance life-time, address issues pertaining to safety of Li-ion batteries and finally provide affordability and cost-competiveness to the envisaged product.
- Solid polymer electrolytes are equally sought after for photo-voltaic devices such

as DSSC and OIHS which are predicted to grow at ~ 40% over the next few decades, high capacity storage and delivery systems.

- An efficient solid electrolyte finds potential applications in LEDs, ECDs, sensors & actuators, etc. with limitless industrial potential.^{1,3,54}

5. References

- (1) Thomas, K. E.; Darling R. M.; Newman, J. In "Advances in Lithium Ion Batteries", Eds. Schalkwijk, W.A. v.; Scrosati, B., Kluwer Academic/Plenum Publishers, NY, 2002; p 345.
- (2) Scrosati, B.; Garche, J. Lithium Batteries, Prospects and Future. *J. Power Sources* **2010**; *195*: 2419–2430.
- (3) Quartarone, E.; Mustarelli, P. Electrolytes for Solid-State Lithium Rechargeable Batteries: Recent Advances and Perspectives. *Chem. Soc. Rev.* **2011**; *40*:2525-2540.
- (4) Gray, F. M. In *Solid Polymer Electrolytes-Fundamentals and Technological Applications*, VCH, Weinheim, Germany, 1991.
- (5) Kleitz, M.; Sapoval, B.; Ravaine, D. Eds. *Solid State Ionics*, North Holland: Amsterdam, 1983.
- (6) Lewis, N. S. Towards Cost-Effective Solar Energy Use. *Science*, **2007**; *315*: 798"801.
- (7) Gratzel, M. Photoelectrochemical Cells. *Nature* **2001**; *414*:338"344.
- (8) Kang, X. Nonaqueous Liquid Electrolytes for Lithium Based Rechargeable Batteries. *Chem. Rev.* **2004**; *104*:4303-4417.
- (9) Scrosati, B.; Croce, F.; Panero, S. Progress in Lithium Polymer Battery R& D. *J. Power Sources* **2001**; *100*:93-100.
- (10) Fenton, D. E.; Parker, J. M.; Wright, P. V. Complexes of Alkali Metal Ions with Poly(ethylene oxide). *Polymer* **1973**, *14*: 589"589.
- (11) Wright, P. V. Electrical conductivity in ionic complexes of poly(ethylene oxide). *Br. Polym. J.* **1975**; *7*: 319"327.
- (12) Wright, P. V. An Anomalous Transition to a Lower Activation Energy for dc Electrical Conduction above the Glass-Transition Temperature. *J. Polym. Sci., Polym. Phys. Ed.* **1976**; *14*: 955"957.
- (13) Armand, M. B.; Chabagno, J. M.; Duclot, M. J. *Extended Abstracts, Second International Conference on Solid Electrolytes*, St. Andrews, Scotland, 1978.
- (14) Armand, M. B.; Chabagano, J. M.; Duclot, M. J. In *Fast Ion Transport in Solids: Electrodes Electrolytes*, Proceedings of the International Conference on Fast Ion Transport in

- Solids, Electrodes, and Electrolytes, Lake Geneva, WI, 1979; May 21"25,
- (15) Vashishta, P., Mundy, J. N., Shenoy, G. K., Eds.; Elsevier/North-Holland: New York, 1979; p 131.
- (16) Ratner, M. A. In *Polymer Electrolyte Reviews-1*; MacCallum, J. R., Vincent, C. A., Eds. Elsevier Applied Science: New York, 1987; Vol. 1.
- (17) MaCallum, J. R.; Vincent, C. A. *Polymer Electrolytes Reviews*; Elsevier: London, 1987 (Vol 1), 1989 (Vol 2).
- (18) Ratner, M. A.; Shriver, D. F. Ion Transport in Solvent-Free Polymers. *Chem. Rev.* **1988**; 88: 109"124.
- (19) Gray, F. M. *Polymer Electrolytes*; The Royal Society of Chemistry: Cambridge, UK, 1997.
- (20) Alamgir, M. Abraham, K. M. In *Lithium Batteries-New Materials, Developments and Perspectives*; Pistoia, G., Ed. Elsevier: Amsterdam, 1994.
- (21) Megahed, S.; Scrosati, B. *The Electrochemical Society Interface* **1995**; 35-37.
- (22) Henricksen, G. L.; De Luca, W. H.; Vissers, D. R. *Chemtech* **1994**; 32-35.
- (23) Ishikawa, R.; Hazama, T.; Mivabashi, M.; Andoh, H. *Proceedings of the International Workshop on Advanced Batteries*; Osaka, Japan, 1995; pp 22-24.
- (24) F. Croce, G. B, Appetecchi, L, Persi, B. Scrosati. *Nature* **1998**;394: 456.
- (25) Acosta, J, L.; Morales, E. *J. Appl.Polym.Sci* , **1996**; 60: 1185.
- (26) Kobayashi, N.; Uchiyama, M.; Shigehera, K.; Tsuchid, E. *J. Phys. Chem.* **1985**; 89: 987.
- (27) Watanabe, M.; Sanui, K.; Ogata. N, Kobayashi, T.; Ohtaki, Z. *J. Appl. Phys.* **1985**; 57: 123.
- (28) Killis, A.; LeNest, J, F; Gandini, A.; Cheradame, H.; Cohen-Added, J, P. *Solid State Ionics* **1984**; 14: 231.
- (29) Andrei, M.; Sorpani, M. *Polymer* **1988**; 39: 7041.
- (30) Sperling L.H, *Interpenetrating polymer networks; Advances in Chemistry Series*; Klemper, D.; Sperling, L, H.; Utrachi, L, A.; Eds.; Washington DC.; 1994.; vol 239.
- (31) Basak, P.; Manorama, S. V. *Solid State Ionics* **2004**; 167: 113"121.
- (32) Basak, P.; Manorama, S. V *Eur. Polym. J.* **2004**; 40: 1155"1162.
- (33) Basak, P.; Manorama, S. V.; Singh, R. K.; Prakash, O. *J. Phys. Chem. B* **2005**; 109: 1174"1182.
- (34) Basak, P.; Manorama, S. V. *J. Macromol. Sci., Pure Appl. Chem.* **2006**; 43: 369"382.
- (35) Basak, P.; Parkash, O.; Chatterji, P. R. *J. Macromol. Sci., Pure Appl.*

- Chem.* **2001**; 38 :399-415.
- (36) Ramanjaneyulu, K.; Bar, N.; Shah, Md. S. A. S.; Manorama, S. V.; Basak, P. *J. Power Sources*, **2012**; 217: 29"36.
- (37) Shah, Md. S. A. S.; Basak, P.; Manorama, S. V. *J. Phys. Chem. C*, **2010**; 114: 14281"14289.
- (38) Bar, N.; Ramanjaneyulu, K.; Basak, P. *J. Phys. Chem. C*. **2014**; 118: 159"174.
- (39) J, R, MacCallum.; C, A, Vincent. (ed), *Polymer Electrolyte Review-I & II*, Elsevier, London, 1987.
- (40) F. Kremer A. Schonhals (Eds.), *Broad Band Dielectric Spectroscopy*, Springer-Verlag Berlin Heidelberg, New York, 2003.
- (41) B, E, Mellander.; I, Albinsson. in *Solid State Ionics: New Developments*, Proceeding of 5th Asian Conference, Chowdari BVR, Dissanayake MAKL, Careem MA (Eds.) **1996**; 83-95.
- (42) L. R. A. K. Bansara, M. A. K. L. Dissanayake, M. Furlani B. E. Mellander. *Ionics*, **2000**; 6 :239.
- (43) M, C, Wintersgill J, J, Fontanella. In *Polymer Electrolyte Review- II*, MacCallum, J, R.; Vincent, C, A.; (ed), Elsevier, London ;1987.
- (44) Di Noto, V. *J. Phys. Chem B*. **2000**; 104: 10116.
- (45) MacCallum, J. R.; Vincent, C. A. In *Polymer Electrolyte Reviews-I*; MacCallum, J. R. Vincent, C. A. Eds. Elsevier Applied Science: New York, **1987**; Vol 1.
- (46) MacDonald, J. R.; Johnson, W. B. In *Impedance Spectroscopy*; MacDonald, J. R., Ed.; J. Wiley & Sons: NewYork, 1987; p23.
- (47) Han, D G.; Choi G. M. *Solid State Ionics*. **1998**; 106: 71.
- (48) Macdonald J R, *Impedance spectroscopy, Emphasizing Solid Materials and Systems*. Wiley, New York, 1987.
- (49) Brug G J, Vanden Eeden ALG, Sluytes-Rehbach M, Sluyters JH, *J. Electroanal. Chem.* **1984**; 176: 275.
- (50) Bellucci F.; Valentino M.; Monetta T.; Nicodemo L.; Kenny J.; Nicolas L.; Mijovic J. *J. Polym. Sci Part B Polym Phys*, **1994**; 32: 2519.
- (51) M. Venkateswaralu, K. Narashima Reddy, B. Rambabu., V Satyanarayana. *Solid State Ionics*. **2000**;127: 177.
- (52) A; K; Jonscher. *Nature*, **1977**, 256, 673 A; K; Jonscher. *J. Mater Sci*; **1981**; 16:2037.
- (53) K, Funke. *Solid State Ionics*, **1997**; 94 :27.
- (54) M. D. Ingram *Phys. Chem. Glasses*, **1987**; 6: 215.